Hutnické listy – *Metallurgical Journal*
Speciální vydání / Special Issue, roč. / vol. LXXIX
ISSN Online: 3029-8350

Optimising Strength in Structural Steel Tubes Via Modelling of the Controlled Cooling Process

Optimalizace pevnosti konstrukčních ocelových trubek pomocí modelování procesu řízeného ochlazování

Nathan Dixon[1], Denzi Li[1], Jinlong Du[2], Carl Slater[1], Claire Davis[1]

[1] WMG, University of Warwick, United Kingdom. *Contact e-mail: N.Dixon.1@warwick.ac.uk
[2] Tata Steel Research and Innovation Ltd, United Kingdom

Abstract

Grain size strengthening predominantly determines the strength of low-carbon low-alloy steel tube grades consisting of a ferrite-pearlite microstructure. While recent changes to standards now permit the use of controlled cooling to refine grain size and enhance mechanical properties, the industrial application of multi-stage controlled cooling lacks robust predictive models. This study developed a finite element (FE) COMSOL-based modelling framework that integrates thermodynamic simulations, phase transformation data, and empirical grain-size relationships to simulate industrial water and air-cooling stages.

The model achieves high predictive accuracy by focusing on the critical undercooling threshold where the first 40% of ferrite forms. Validation against industrial production data yielded a root mean square error (RMSE) of 6.5 MPa for ultimate tensile strength. Furthermore, a parametric study of 22 cooling configurations demonstrates that optimised processing can achieve a 5% strength uplift for specific geometries while successfully avoiding undesirable bainite formation. This framework provides a robust tool for manufacturers to improve process control, product design, and mechanical performance.

***Keywords**: controlled cooling, steel tube manufacturing, ferrite grain size control, FE modelling, phase transformation, process optimisation*

Abstrakt

Pevnost trubek z nízkouhlíkových nízkolegovaných ocelí s ferit-perlitovou mikrostrukturou je převážně určena velikostí zrna. Ačkoli nedávné změny norem nyní umožňují využití řízeného ochlazování ke zjemnění zrna a zlepšení mechanických vlastností, pro průmyslové uplatnění vícestupňového řízeného ochlazování dosud neexistují spolehlivé prediktivní modely. V této studii byl vyvinut modelovací rámec založený na metodě konečných prvků (FE) v prostředí COMSOL, který integruje termodynamické simulace, data o fázových přeměnách a empirické vztahy velikosti zrn pro simulaci průmyslových fází chlazení vodou a vzduchem. Model dosahuje vysoké prediktivní přesnosti díky zaměření na kritickou prahovou hodnotu podchlazení, při níž se tvoří prvních 40% feritu. Ověření na základě průmyslových výrobních dat vykázalo chybu střední kvadratické odchylky (RMSE) 6,5 MPa pro mez pevnosti v tahu. Parametrická studie 22 konfigurací chlazení dále ukazuje, že optimalizovaným zpracováním lze u specifických geometrií dosáhnout zvýšení pevnosti o 5% a současně úspěšně zabránit nežádoucí tvorbě bainitu. Tento rámec poskytuje výrobcům robustní nástroj pro zlepšení řízení procesů, návrhu produktů a mechanických vlastností.

***Klíčová slova:** řízené ochlazování, výroba ocelových trubek, řízení velikosti zrn feritu, modelování metodou konečných prvků, fázová transformace, optimalizace procesu*

Hutnické listy – *Metallurgical Journal*
Speciální vydání / Special Issue, roč. / vol. LXXIX
ISSN Online: 3029-8350

1. Introduction

Structural steel tubes in the EN S355-S460 range are widely used in structural applications that demand reliable combinations of strength and ductility. These grades are designed to achieve yield strengths between 355 MPa and 460 MPa, with corresponding ultimate tensile strengths ranging from 470 MPa to 720 MPa [1]. The typical chemical composition of steel grade S355 is shown below in **Tab. 1**. These tubes consist of ferrite-pearlite microstructures and primarily derive strength from the ferrite grain size formed during cooling after tube shaping. A ferrite-pearlite microstructure is targeted for these products, as the presence of bainite or martensite can lead to undesirable variability in mechanical performance. With recent changes to standards now permitting controlled cooling rather than continuous cooling [1], opportunities have emerged to refine ferrite grain size and enhance mechanical properties further. Ensuring that tubes remain within the correct transformation regime during cooling is therefore essential for achieving the required and consistent strength levels.The present study develops and validates a modelling framework that integrates thermophysical simulation, CCT-based phase transformation prediction and empirical grain-size relationships to support optimisation of cooling strategies [8] in industrial tube production.

Tab. 1 Typical chemical composition of steel grade S355 [1]
Tab. 1 Typické chemické složení ocelové třídy S355 [1]

Grade	C max. (Wt%.)	Si max. (Wt%.)	Mn (Wt%.)	Nb max. (Wt%.)
S355	0.2	0.5	0.9 – 1.65	0.05

Previous modelling efforts have mainly focused on the thermodynamic modelling of hot rolling [2], forming [3], continuous cooling of tubes [4] and rapid quenching [5]. To date, no existing models investigate the multi-stage controlled cooling of tubes to predict both thermal history and product properties. To achieve a model of this production process, consideration of thermal history, phase transformation and microstructure are required.

1.1 Tube Manufacturing

The final mechanical properties of structural steel tubes are established during a two-stage controlled cooling process applied immediately after tube forming and annealing. Initially, tubes are annealed at temperatures ranging from 850 °C to 1000 °C for durations ranging from 18 to 30 minutes [6-8]. This stage ensures the development of a uniform austenite microstructure prior to transformation. After annealing, water cooling is used to rapidly lower the tube temperature; these cooling rates can span 0.3 °C/s to 50 °C/s [9, 10], depending on product geometry. During this water-cooling stage, the aim is to form ferrite under high undercooling conditions. Water cooling brings the tube down to temperatures above the bainite formation region, generally between 550 °C and 600 °C. Once the appropriate temperature range has been reached, tubes are slowly air cooled down to room temperature (at rates ranging from 0.06 °C/s-0.9 °C/s) [4, 11]. Due to variations in geometry, wall thickness, line speed, and cooling configuration, the industrial cooling profile varies significantly across the tube's perimeter and through its thickness [12]. The typical thermal profile range experienced industrially can be seen in **Fig. 1**. Understanding the thermal profiles generated industrially and the potential variations are essential for understanding and predicting the resulting microstructure and mechanical properties.

Hutnické listy – *Metallurgical Journal*
Speciální vydání / Special Issue, roč. / vol. LXXIX
ISSN Online: 3029-8350

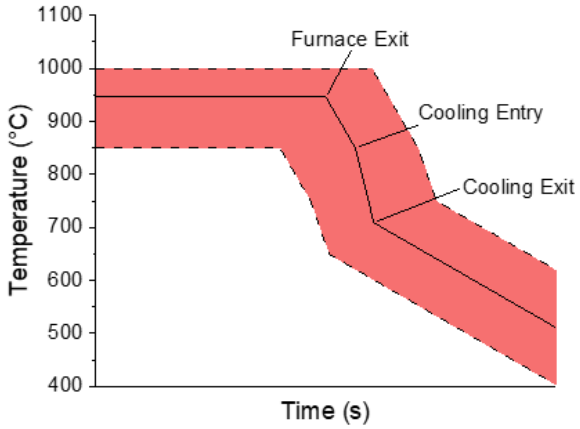

Fig. 1 Typical thermal profile experienced during tube manufacturing

Obr. 1 Typický teplotní profil při výrobě trubek

1.2 Grain Size Control During Controlled Cooling

Ferrite grain size plays a critical role in determining the mechanical properties of S-grade structural steels, contributing as much as 60% of the final yield strength [13]. Grain refinement is typically promoted by high cooling rates to achieve increased undercooling, which influences the balance of ferrite nucleation and growth [14]. A previous experimental study has established that during controlled cooling, a strong correlation exists between the ferrite grain size and the undercooling at which the initial 40% ferrite forms [15]. This empirical relationship can be seen in Eq. (1), where $\Delta T_{40\%}$ is the undercooling at which 40% ferrite forms. This equation is known to apply for an austenite grain size, dγ, of 10 μm.

$$d_\alpha = 0.71 \cdot d_\gamma \cdot e^{-0.0038 \cdot \Delta T_{40\%}} \quad (1)$$

Within the initial 40% of ferrite formation, the consumption or saturation of nucleation sites within the initial 40% of ferrite formation prevents further nucleation, thereby determining the final grain size. To maximise the degree of achievable ferrite refinement, the undercooling within this initial 40% of ferrite formation should be maximised. Achieving sufficient undercooling to refine the grain size, whilst simultaneously avoiding entry into the bainitic transformation range, is therefore essential for achieving the required strength levels.

However, to gain an understanding of the ferrite grain sizes produced during industrial controlled cooling, the 40% undercooling needs to be known. A solution to identifying these values is a finite element model of the tube manufacturing to predict thermal history and phase fraction.

2. Aims

The primary objective of this work is to develop a finite element (FE) COMSOL based model capable of simulating the controlled cooling process used during the manufacture of structural steel tubes. The model aims to predict the thermal history of tubes subjected to a wide range of industrial cooling conditions and to use these predictions to estimate ferrite grain size and resultant mechanical properties.

Hutnické listy – *Metallurgical Journal*
Speciální vydání / Special Issue, roč. / vol. LXXIX
ISSN Online: 3029-8350

By integrating thermodynamic and phase transformation models alongside empirical grain size and mechanical property relationships, the model should provide a framework for evaluating and optimising cooling strategies. Ultimately, the goal is to identify cooling conditions that can deliver improved strength levels across different tube geometries and thicknesses, supporting the development of improved efficiency, higher-performance cooling strategies.

3. Modelling Methodology

3.1 Tube production process

The tube production process (see **Fig. 2**) begins with annealing, where the tube is heated to achieve the desired austenite microstructure. Post annealing, tubes are subsequently descaled and formed into their final rectangular geometry. Prior to forming, tubes are circular with a radius of 20 inches (508 mm), the shaping from circular to rectangular induces negligible strain, which is not expected to noticeably influence phase transformation. Tubes are then cooled using eight cooling banks to achieve a targeted exit temperature (above the bainite formation region). Each cooling bank utilises multiple nozzles to achieve a uniform reduction in temperature around the tube perimeter, as illustrated by the nozzle arrangement in the inset diagram. After water cooling, tubes are left on the run-out table.

Temperature is measured at key points using pyrometers located at the furnace exit, cooling entry, and cooling exit. The temperature-time plot from those pyrometer readings was shown earlier in **Fig. 1**, which demonstrates the range of thermal profiles that can be generated via processing parameter variation.

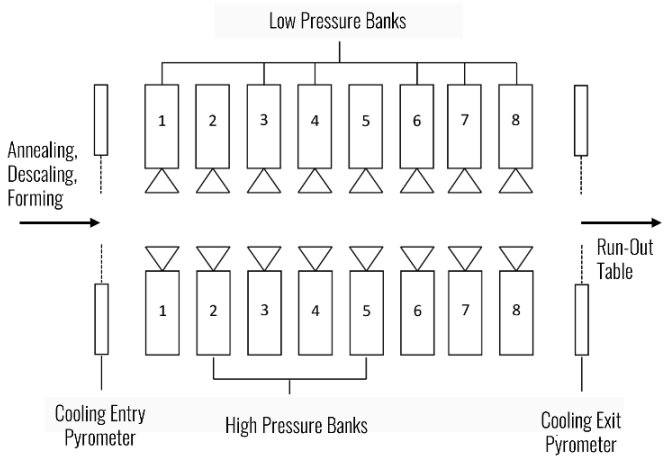

Fig. 2 Schematic showing the tube manufacturing process with cooling banks emphasised

Obr. 2 Schéma znázorňující proces výroby trubek s vyznačenými chladicími sekcemi

3.2 Model Setup

For the investigation of this topic, an FE model was developed using COMSOL (version 6.3) to capture the thermal and microstructural behaviour of tubes during production. The model integrates a comprehensive set of geometric and process inputs. These are supplemented by material-specific data, as well as physical properties sourced from JMatPro (version 15.1) which include temperature dependent material properties. Another export from JMatPro includes CCT / TTT data for the S355 alloy.

Hutnické listy – *Metallurgical Journal*
Speciální vydání / Special Issue, roč. / vol. LXXIX
ISSN Online: 3029-8350

These inputs are used to produce a thermal profile and phase fraction, from which the ferrite grain size can be determined. Once grain size is determined, mechanical properties such as yield and ultimate tensile strength can be derived. A flow chart illustrating the inputs and outputs of the FE model is shown below in **Fig. 3.**

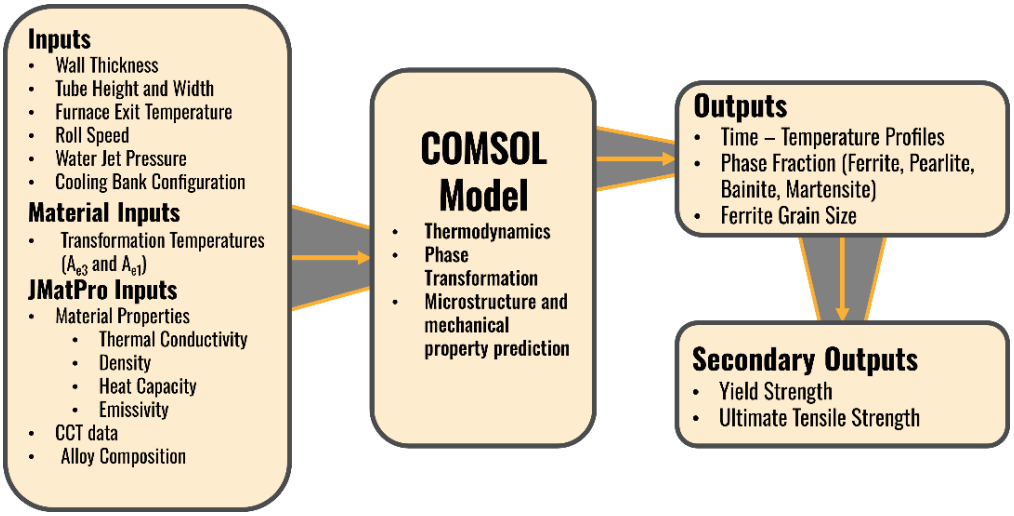

Fig. 3 Flow chart demonstrating the inputs and outputs of the FE model

Obr. 3 Schéma znázorňující vstupy a výstupy modelu konečných prvků

Building on the defined model setup, the simulation focuses on a 2D quarter cross-section of a rectangular tube, capturing its behaviour from the furnace exit through to the run-out table. The cooling process is represented using a combined approach that accounts for water-jet cooling as well as heat losses through radiation and convection, as illustrated by the boundary-condition layout (see **Fig. 4**). Latent heat is also included as a heat source within the material bulk. Within **Fig. 4**, the model meshing can be seen where a finer mesh is utilised in the regions where industrial tensile tests would be taken from. Where no industrial data is available, a coarser meshing is utilised.

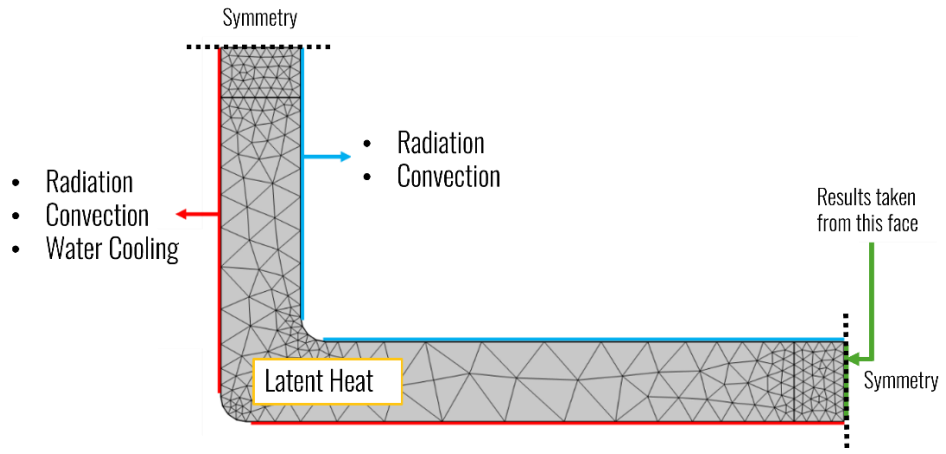

Fig. 4 Boundary-condition and meshing setup for the numerical model of tube cooling. Future results are taken from average along the face indicated

Obr. 4 Okrajové podmínky a nastavení sítě pro numerický model chlazení trubek. Budoucí výsledky jsou převzaty z průměru podél vyznačené plochy

Hutnické listy – *Metallurgical Journal*
Speciální vydání / Special Issue, roč. / vol. LXXIX
ISSN Online: 3029-8350

3.3 Heat Transfer Coefficients

The modelling of heat extraction within the cooling section relies on a detailed description of the heat transfer coefficients (HTCs) associated with both water cooling and radiative-convective losses. For water cooling, eight cooling banks are modelled, with each capable of operating in four distinct modes ranging from 'off' to high-pressure conditions or additional nozzles being activated. Water pressure is linked to nozzle flow rate via an industrially derived empirical relationship, which then determines the variable heat transfer coefficient, H_{water}, used to simulate water cooling.

Fig. 5A illustrates an example of the water-cooling heat transfer coefficient applied over time. The water cooling coefficients were derived from fitting to industrial pyrometer readings, where the range of values are consistent with those reported in the literature, which can range from 400 W/m²°C to 3500 W/m²°C in similar systems [16-18]. For the flow rates and temperature ranges anticipated in this production process, Viscorova et al indicated that the heat transfer coefficient should be within the 1000 W/m²°C to 2000 W/m²°C range [17].

Radiative and convective heat losses are treated separately, with the heat transfer coefficient used for radiation, H_{rad}, expressed through an emissivity-based surface to ambient radiation formula (Eq. (2)), where emissivity, ε, is 0.6. Convection, H_{conv}, (Eq. (3)) is described using an empirical relationship dependent on roll speed, R, and surface temperature [19]. Dry surfaces are modelled using the sum of both radiative and convective heat transfer coefficients.

$$H_{rad} = \varepsilon \cdot k \cdot (T^2 + T_{atm}^2) \cdot (T + T_{atm}) \tag{2}$$

$$H_{conv} = 5.5 \cdot R^{0.926} + \frac{(-3038 + 0.954 \cdot T + 2.14 \cdot 10^{-8} \cdot T^4)}{T - 20} \tag{3}$$

$$H_{dry} = H_{rad} + H_{conv} \tag{4}$$

Fig. 5B shows the temperature dependent H_{dry} coefficients for both the inner and outer walls. For the outer wall H_{dry} value, a fitting parameter is added to the radiative and convective components, resulting in higher cooling intensities than the inner wall. Published values for these mechanisms span from 50 W/m²K to 150 W/m²K [3], aligning well with the model's parameters.

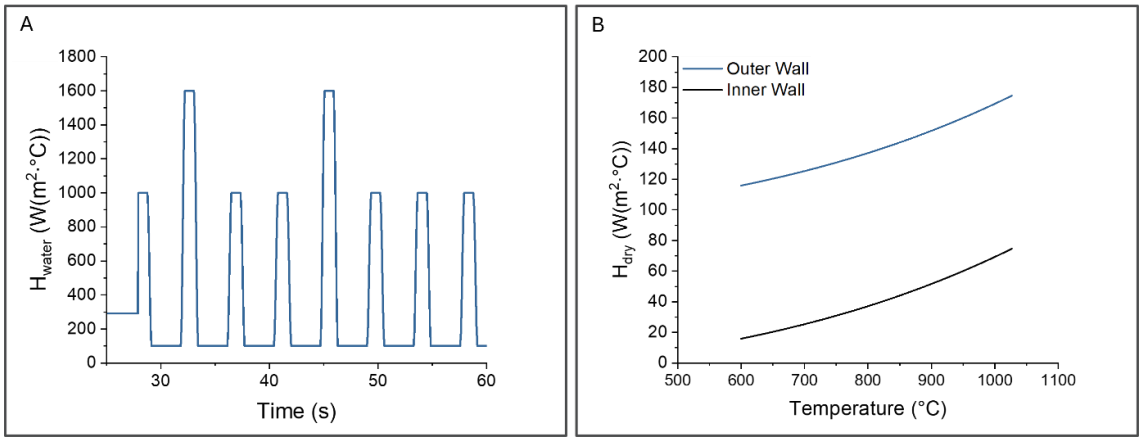

Fig. 1 Heat-transfer coefficients for (A) water cooling and (B) radiative-convective heat exchange applied in the cooling model

Obr. 5 Koeficienty přenosu tepla pro (A) vodní chlazení a (B) radiačně-konvekční výměnu tepla použité v chladicím modelu

Hutnické listy – *Metallurgical Journal*
Speciální vydání / Special Issue, roč. / vol. LXXIX
ISSN Online: 3029-8350

Fig. 6A illustrates an example through-thickness thermal gradient that develop during cooling. It can be seen that significantly faster cooling is experienced at the surface and progressively slower cooling are seen towards the tube centre (inner wall). Near-surface regions typically cool more rapidly, promoting finer ferrite grains and higher strength, however the surfaces are more prone to the risk of bainite formation. The centre experiences slower cooling and correspondingly coarser ferrite-pearlite microstructures. This through-thickness heterogeneity must be considered when designing cooling strategies and whilst predicting mechanical performance. In **Fig. 6A,** Industrial pyrometer readings are superimposed over the model predictions to illustrate the agreement between the model and measured values.

Fig. 6B shows the agreement between the predicted and average measured cooling rig exit temperature for twelve industrial cooling strategies. The error bars indicate a 5% error that may occur in the pyrometer measurement industrially from steam interference, where 5% is estimated from the results of Trofimov et al [20]. It is well known that pyrometer readings can be strongly influenced by steam and surface condition, and the error in measurement can be as extreme as ± 100 °C [21, 22].

The model predicts with a root mean square error (RMSE) accuracy of 23.6 °C, with most data points agreeing with the industrial pyrometer readings. The low accuracy of the pyrometer readings makes it a less reliable metric for model fitting. As a result, the HTC values have been fitted to mechanical property predictions. A greater quality thermal prediction could be made with a more complex cooling model that accounts for more factors. However, the current model attempts to simplify the cooling due to a lack of available knowledge regarding the water-steel interface, water behaviour, water temperature and surface/oxide condition.

To avoid the difficulties of achieving an accurate thermal profile, the heat transfer coefficients used were fitted to mechanical property data as opposed to pyrometer readings. The quality of these mechanical property predictions will be discussed later. In the next sections, the phase transformation and mechanical property predictions will be discussed.

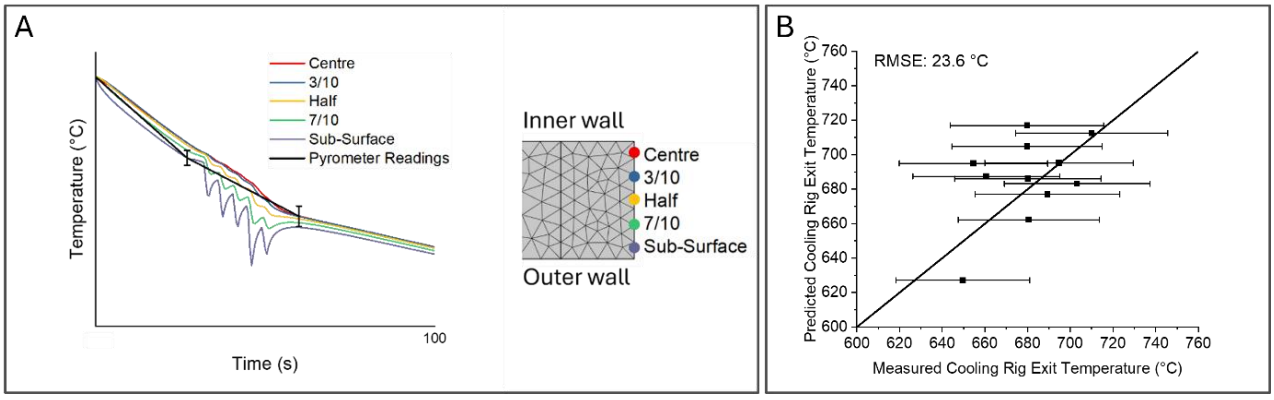

Fig. 2 (A) Example through thickness temperature profiles during cooling. (B) Predicted against measured cooling rig exit temperature

Obr. 6 (A) Příklad teplotních profilů v tloušťce materiálu během ochlazování. (B) Porovnání predikované a naměřené teploty na výstupu z chladicího zařízení

Hutnické listy – *Metallurgical Journal*
Speciální vydání / Special Issue, roč. / vol. LXXIX
ISSN Online: 3029-8350

3.4 Phase Transformation Model

Once a thermal model is established, to make predictions of grain size and mechanical properties, a phase transformation model is necessary to establish a prediction of the formation of 40% ferrite. The phase transformation model used in this study integrates thermodynamic and kinetic data of ferrite formation to establish the phase fractions formed throughout transformation.

Fig. 7A shows schematic of the austenite decomposition via a continuous cooling transformation (CCT) diagram produced by JMatPro that illustrates the onset of ferrite, pearlite and bainite formation under various cooling rates. The imposed cooling profile, plotted in red, intersects the ferrite transformation region at the point where 40% ferrite is formed, denoted as $T_{40\%}$. This temperature is central to predicting the subsequent grain size and strength predictions.

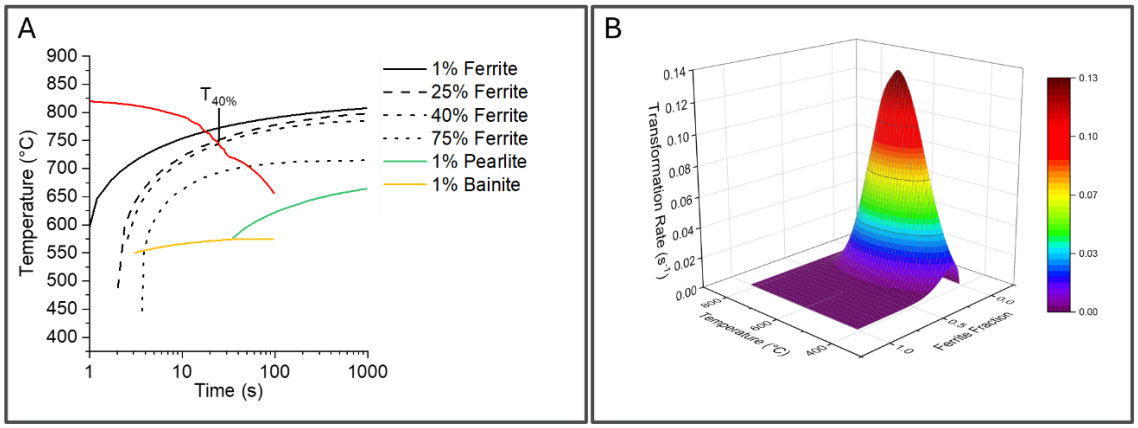

Fig. 3 (A) A continuous cooling transformation (CCT) diagram with superimposed example cooling profile. (B) Temperature and phase fraction dependent transformation rates predicted by JMatPro

Obr. 7 (A) CCT diagram kontinuálního ochlazování s příkladem chladicího profilu. (B) Rychlosti fázových transformací v závislosti na teplotě a fázovém podílu predikované programem JMatPro

The thermal behaviour is translated into a phase transformation prediction using JMatPro transformation rate data, shown in **Fig. 7B.** The current timestep ferrite phase fraction, $F_{\alpha\ new}$, is calculated based on the transformation rate, ΔF_α, which is based on the temperature and the previous time steps fraction transformed, F_α. The equation used to calculate the ferrite fraction at each time step is shown in Eq. (5).

$$F_{\alpha\ new} = F_\alpha + dt \cdot \Delta F_\alpha \tag{5}$$

Once the phase fraction is established, the subsequent step is to translate the 40% ferrite formation temperature into a grain size prediction and hence a mechanical property prediction. This is done via the following steps.

To quantify the driving force for ferrite transformation, the model calculates the undercooling ($\Delta T_{40\%}$) relative to the ferrite-austenite equilibrium temperature, A_{e3}, which is 822 °C for this alloy.

$$\Delta T_{40\%} = A_{e3} - T_{40\%} \tag{6}$$

To predict final mechanical properties, the final ferrite grain size, d_α, needs to be known. d_α is calculated using Eq. (1).

Hutnické listy – *Metallurgical Journal*
Speciální vydání / Special Issue, roč. / vol. LXXIX
ISSN Online: 3029-8350

The solid solution strengthening contribution is calculated using the following equation [23] (where alloying additions are given in weight percentage):

$$\sigma_{SS} = 84 \cdot Si + 32 \cdot Mn + 680 \cdot P + 43 \cdot Ni + 38 \cdot Cu \quad (7)$$

The predicted ferrite grain size and solid-solution term are then combined with a Hall-Petch formula to estimate the yield strength, σ_{YS}, where σ_0 is the friction stress of iron [24, 25]. The ultimate tensile strength, σ_{UTS}, is calculated using a yield strength to ultimate tensile strength conversion value, J, based on industrial data.

$$\sigma_{YS} = \sigma_{SS} + \sigma_0 + 18.1 \cdot d_\alpha^{-0.5} \quad (8)$$

$$\sigma_{UTS} = J \cdot \sigma_{YS} \quad (9)$$

These relations establish a direct link between thermal profile, microstructure and final mechanical properties.

The incorporated JMatPro-based phase transformation model provides a comprehensive description of ferrite formation during multi-stage controlled cooling. As shown in **Fig. 8**, transformation behaviour is sensitive to the thermal history, with ferrite nucleation and growth occurring across a range of temperatures depending on the cooling strategy chosen. This variability directly influences the final ferrite grain size and consequently, the mechanical properties discussed in the preceding subsection.

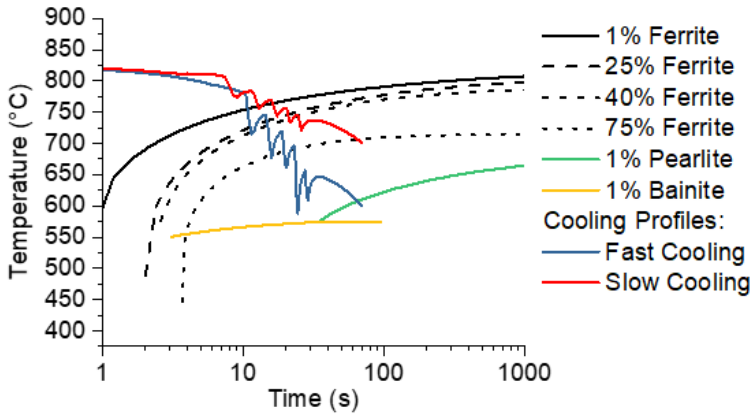

Fig. 4 JMatPro produced CCT with superimposed 'fast' and 'slow' thermal profiles

Obr. 8 JMatPro modul pro znázornění CCT diagram s možností překrytí "rychlých" a "pomalých" teplotních profilů

The CCT diagram in **Fig. 8** includes several ferrite start curves (0-75% transformation) together with pearlite and bainite start curves. Two representative cooling profiles, one 'fast' and one 'slow' simulated thermal profiles are superimposed to illustrate maxima and minima cooling strategies. Under 'fast' cooling, the thermal profile is predicted to cross the 40% ferrite formation temperature at approximately 715 °C, resulting in an undercooling of around 107 °C, leading to the formation of fine ferrite grains of around 4.7 μm.

Conversely, 'slow' cooling intersects the ferrite region at higher temperatures (≈ 740 °C), promoting coarser ferrite (≈ 5.2 μm) due to lower undercoolings (≈ 82 °C) and hence lower nucleation rates.

Hutnické listy – *Metallurgical Journal*
Speciální vydání / Special Issue, roč. / vol. LXXIX
ISSN Online: 3029-8350

In addition to differences imposed by the overall cooling rate, local variations in transformation behaviour are expected through the thickness of industrially processed product, which will lead to a through thickness distribution of grain sizes and hence strengths.

By integrating experimentally derived CCT data with the transformation model, the methodology enables prediction of microstructural evolution for cooling strategies. The combination of transformation kinetics, grain-size estimation, and composition-based strengthening models forms a consistent foundation for the strength predictions discussed in the next sections of the article.

4. Results and Discussion

4.1 Model Validation

The model was validated against twelve industrial data points representatives of commercially produced structural steel tube, covering a wide range of cooling profiles, geometries, wall thicknesses and annealing conditions. The comparison between predicted and measured average ultimate tensile strength is shown in **Fig. 9**. The predicted strength is taken from the measurement point is indicated in **Fig. 4,** where the inner and outer 1 mm are excluded from measurement. The Y-axis error bars are indicative of the error present in Eq. (1) [15]. The X-axis error bars indicate the ranges of industrial measurements. Model predictions for UTS align closely with industrial measurements, yielding an RMSE of 6.5 MPa. These results demonstrate that the integrated transformation and grain-size modelling approach provides accurate predictions for the S355 grade studied. The close clustering of data points around the one-to-one line highlights the ability of the model to reliably capture the influence of cooling strategy on ferrite transformation and resulting strength. The validation also confirms that JMatPro-based phase transformation predictions provide adequate fidelity for grain-size estimation across the tested conditions. With this level of accuracy, the model can be confidently used as a tool to support the selection and optimisation of processing parameters in industrial tube production.

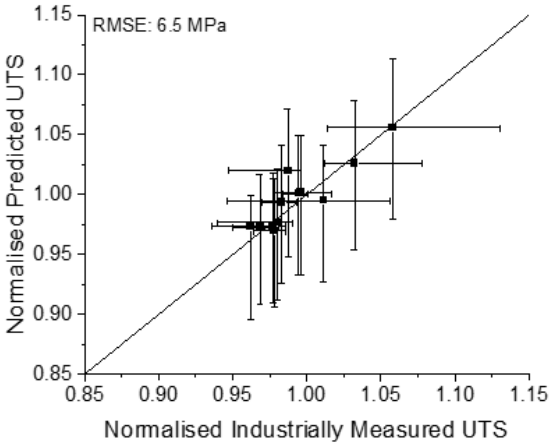

Fig. 5 Model validation plot comparing normalised predicted UTS with normalised industrially measured UTS (RMSE = 6.5 MPa)

Obr. 9 Graf ověření modelu porovnávající normalizovanou predikovanou mez pevnosti v tahu s normalizovanou průmyslově naměřenou mezí pevnosti v tahu (RMSE = 6,5 MPa)

The measured normalised yield and ultimate tensile strengths are plotted, in **Fig. 10**, against the predicted values, with bainite formation predictions shown.

Hutnické listy – *Metallurgical Journal*
Speciální vydání / Special Issue, roč. / vol. LXXIX
ISSN Online: 3029-8350

The predicted values include twenty two cooling strategies, with three annealing temperatures, two tube geometries and three strip thicknesses. These cooling strategies are deemed to be representative of the full range of industrial processing conditions. Industrial data includes multiple measurements per tube.

It can be seen that the model predicts the mechanical properties reasonably well for a wide range of products, encompassing the UTS values for most tubes produced commercially. The UTS predictions span from 0.94 to 1.05, encompassing almost the full range of UTS values produced by ferrite-pearlite microstructures. For yield strengths, the industrial data is more scattered than the UTS data. Due to the model using a linear yield strength to UTS ratio, Eq. (9), a lower range of yield strengths are predicted by the model. However, the model still encompasses around 60% of the yield strength range. Given a set of processing parameters, the model is capable of providing a reasonable prediction of the final mechanical properties in a wide range of S355 tube products.

The model also predicts the onset of bainite formation well. The onset of bainite formation marks the upper limit for the predictive range of the model, since no bainite strengthening contribution is calculated. The model conditions where bainite forms align with the point at which the linear yield to UTS ratio breaks down industrially, which is representative of the transition from ferrite-pearlite to ferrite-bainite microstructures, this is marked by the box in **Fig. 10**. The accurate prediction of bainite formation supports the assumptions made for the thermal and phase transformation models and demonstrates that they are sufficient for the current needs. The ability to predict bainite formation allows for appropriate processing conditions to be selected to form high strength ferrite-pearlite microstructures, which will be discussed in the subsequent section.

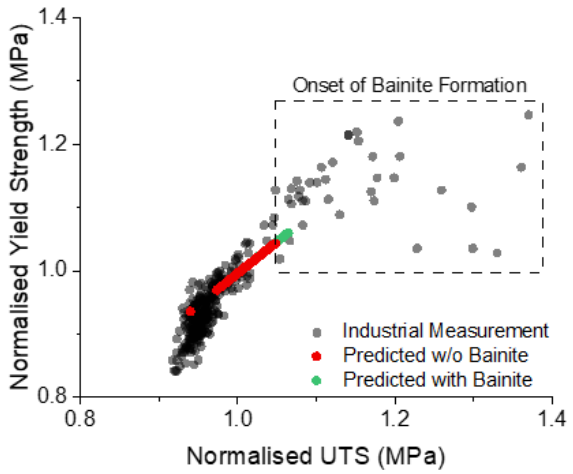

Fig. 10 Normalised yield strength against normalised ultimate tensile strength with both industrial data and model predictions plotted. The onset of bainite formation is indicated

Obr. 10 Normalizovaná mez kluzu v závislosti na normalizované mezní pevnosti v tahu; v grafu jsou znázorněna jak průmyslová data, tak modelové predikce. Je vyznačen počátek tvorby bainitu

4.2 Optimisation of Cooling Parameters

Using the validated framework, a parametric study was conducted to assess the levels of strength improvement possible using current industrial equipment. Twenty two cooling strategies with varying cooling bank configurations, nozzle configurations and pressures were tested for a single product geometry annealed at 900 °C.

Hutnické listy – *Metallurgical Journal*
Speciální vydání / Special Issue, roč. / vol. LXXIX
ISSN Online: 3029-8350

Three example cooling strategies are shown in **Fig. 11A** alongside the normalised UTS strengths predicted from each cooling strategy in **Fig. 11B**. The parametric study demonstrates that a 5% increase in strength is achievable for this specific geometry through optimised parameter selection.

	Low	Medium	High
Bank 1	Off	Off	Off
Bank 2	Off	On	On
Bank 3	Off	On	On
Bank 4	Off	On	On
Bank 5	Off	On	On
Bank 6	Off	On	On
Bank 7	Off	On	On
Bank 8	Off	Off	Off
High Pressure Valve 1	Off	On	On
High Pressure Valve 2	Off	On	On
Bank 1 Extra Nozzles	Off	Off	Off
Bank2 Extra Nozzles	Off	Off	Off
Bank3 Extra Nozzles	Off	On	On
Bank4 Extra Nozzles	Off	On	On
Bank5 Extra Nozzles	Off	Off	On
Bank6 Extra Nozzles	Off	Off	On
Bank7 Extra Nozzles	Off	Off	Off
Bank8 Extra Nozzles	Off	Off	Off

Tube Height (mm)	Tube Width (mm)	Wall Thickness (mm)	Annealing Temperature (°C)
150	250	10	900

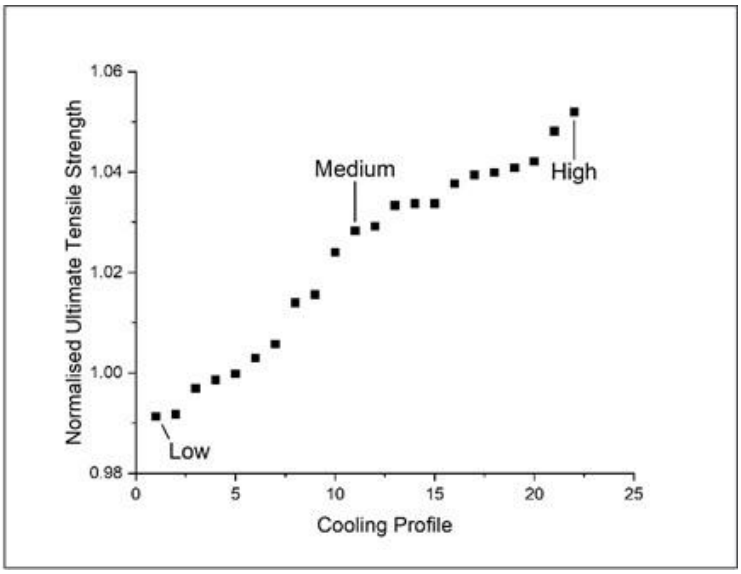

Fig. 11 Effect of cooling-parameter configurations on the predicted normalised ultimate tensile strength

Obr. 11 Vliv nastavení parametrů chlazení na predikovanou normalizovanou mez pevnosti v tahu

The present FE model offers the opportunity to map the processing capabilities of the current manufacturing routes whilst providing manufacturers the opportunity for process optimisation and control.

5. Conclusions

During this study, a thermal FE model which utilises thermodynamic and phase transformation modelling with integrated empirical relationships to predict microstructural features (ferrite grain size) and mechanical properties has been established.

The model has been developed to replicate a typical structural steel tube production process and simulates from annealing via controlled cooling through to the run-out table. The present study provides greater understanding of the thermal histories generated throughout controlled cooling and the resultant mechanical properties.

The key findings from this study are as follows:

- The model generates thermal profile predictions that align closely with industrial pyrometer measurements. Processing parameter inputs, including processing parameters, product geometry and chemical composition can be varied to produce a range of thermal profile predictions. The cooling bank exit temperature is predicted with an RMSE accuracy of ± 23.6 °C.
- The model uses thermodynamic, phase transformation prediction and empirical relationships to establish an accurate prediction of final mechanical properties, namely ultimate tensile strength. An RMSE accuracy of ± 6.5 MPa.

Hutnické listy – *Metallurgical Journal*
Speciální vydání / Special Issue, roč. / vol. LXXIX
ISSN Online: 3029-8350

- The model predictions for the onset of bainite formation are aligned with industrial data. Allowing for processing parameters to selected to avoid ferrite-bainite microstructures.
- The high accuracy of the UTS predictions, substantiates the methodology used for microstructural and phase transformation modelling.
- A parametric study was conducted to assess the potential for strength improvements via optimised processing parameter selection. A select finding from this work is that by adjusting cooling bank parameters, a potential 5% strength uplift can be achieved, this value will vary between products and will be investigated further.

Reference

[1] Institution, B.S., Hot finished structural hollow sections of non-alloy and fine grain steels. 2006, BSI.
[2] Langbauer, R., et al., Investigation of the temperature distribution in seamless low-alloy steel pipes during the hot rolling process. Advances in Industrial and Manufacturing Engineering, 2021. **2**: p. 100038.
[3] Chen, D., et al., Online cooling system and improved similar self-adaptive strategy for hot-rolled seamless steel tube. ISIJ International, 2021. **61**(7): p. 2135-2142.
[4] Souza, J.L.F., M. Ziviani, and J.F.A. Vitor, Mathematical modelling of tube cooling in a continuous bed. Applied Thermal Engineering, 2015. **89**: p. 80-89.
[5] Gomes, D.F., R.P. Tavares, and B.M. Braga, Mathematical model for the temperature profiles of steel pipes quenched by water cooling rings. Journal of materials research and technology, 2019. **8**(1): p. 1197-1202.
[6] Landfahrer, M., et al., Characterization of the temperature distribution on steel tubes for different operating conditions in a reheating furnace using CFD and three different measuring methods. Applied Thermal Engineering, 2018. **133**: p. 39-48.
[7] Raič, J., et al., Modelling of the cooling process of steel tubes in a rake type cooling bed. Applied Thermal Engineering, 2020. **169**: p. 114895.
[8] Landfahrer, M., et al., Development of a numerically efficient CFD model to predict transient temperature distribution of mother tubes moving translative and rotative through a gas fired furnace. Applied Thermal Engineering, 2017. **123**: p. 290-300.
[9] Manohar, P.A. and T. Chandra, Continuous cooling transformation behaviour of high strength microalloyed steels for linepipe applications. ISIJ international, 1998. **38**(7): p. 766-774.
[10] Amirjani, N., M. Ketabchi, M. Eskandari, and M. Hizombor, Effect of cooling rate and finish rolling temperature on structure and strength of API 5LX70 linepipe steel plate. Journal of Materials Engineering and Performance, 2020. **29**: p. 4275-4285.
[11] Souza, J.L.F., et al., Experimental Measurementt of Internal Temperature of a Tube in Cooling on a Bed of Passage, Continuous Under Natural Convection. Thermal Engineering, 2019. **18**(2): p. 06-12.
[12] Brunbauer, S., et al., Residual stress and microstructure evolution in steel tubes for different cooling conditions – Simulation and verification. Materials Science & Engineering A, 2019. **747**: p. 73-79.
[13] Tovee, J.P., Microstructural Influence On The Effects Of Forward And Reverse Mechanical Deformation In Hsla X65 And X80 Linepipe Steels, in Department of Metallurgy and Materials. 2014, University of Birmingham.
[14] Militzer, M., R. Pandi, and E.B. Hawbolt, Ferrite nucleation and growth during continuous cooling. 1996. **27**: p. 1547-1556.
[15] Dixon, N., C. Slater, J. Du, and C. Davis, Determination of Final Ferrite Grain Size During Multiple-Stage Controlled Cooling of Low-Carbon, Low-Alloy Steels. Metals, 2025. **15**(9): p. 956.
[16] Wendelstorf, J., K.-H. Spitzer, and R. Wendelstorf, Spray water cooling heat transfer at high temperatures and liquid mass fluxes. International Journal of heat and mass transfer, 2008. **51**(19-20): p. 4902-4910.
[17] Viscorova, R., R. Scholz, K. Spitzer, and J. Wendelstorf, Spray water cooling heat transfer under oxide scale formation conditions. Advanced Computational Methods in Heat Transfer IX, 2006. **53**: p. 163-172.
[18] Wang, H., W. Yu, and Q. Cai, Experimental study of heat transfer coefficient on hot steel plate during water jet impingement cooling. Journal of Materials Processing Technology, 2012. **212**(9): p. 1825-1831.
[19] Edalatpour, S., A. Saboonchi, and S. Hassanpour, Effect of phase transformation latent heat on prediction accuracy of strip laminar cooling. Journal of Materials Processing Technology, 2011. **211**(11): p. 1776-1782.
[20] Trofimov, A.A., et al., Infrared thermometry in high temperature materials processing: influence of liquid water and steam. Quantitative InfraRed Thermography Journal, 2023. **20**(3): p. 123-141.
[21] Huang, Y., et al., Experimental investigation on the effects of particulate interference on radiation thermometry. International Journal of Heat and Mass Transfer, 2024. **224**: p. 125350.
[22] Sugiura, M., et al., Two-color method for steel temperature measurement unaffected by water-induced obstructions. ISIJ International, 2023. **63**(2): p. 346-353.
[23] Gladman, T., Physical metallurgy of microalloyed steels. (No Title), 1997.
[24] Petch, N., The upper yield stress of polycrystalline iron. Acta Metallurgica, 1964. **12**(1): p. 59-65.
[25] Baker, T.N., Microalloyed Steels. Ironmaking and Steelmaking, 2016. **43**(4): p. 267 - 307.